ACS APPLIED MATERIALS & INTERFACES

Research Article

www.acsami.org

Electron Transport Dynamics in TiO_2 Films Deposited on Ti Foils for Back-Illuminated Dye-Sensitized Solar Cells

Liang-Che Chen,[†] Chien-Te Hsieh,*[,‡] Yuh-Lang Lee,[†] and Hsisheng Teng*[,†,§]

[†]Department of Chemical Engineering and Research Center for Energy Technology and Strategy, National Cheng Kung University, Tainan 70101, Taiwan

[‡]Department of Chemical Engineering and Materials Science, Yuan Ze Fuel Cell Center, Yuan Ze University, Taoyuan 32023, Taiwan

[§]Center for Micro/Nano Science and Technology, National Cheng Kung University, Tainan 70101, Taiwan

Supporting Information

ABSTRACT: In this study, we examine the electron transport dynamics in TiO_2 films of back-illuminated dye-sensitized solar cells. The TiO_2 films are fabricated using electrophoretic deposition (EPD) and the conventional paste-coating (PC) of TiO_2 nanoparticles on Ti-foil substrates. Intensity-modulated photocurrent spectroscopy reveals that red-light irradiation is more efficient than blue-light irradiation for generating photocurrents for back-illuminated cells. A single trapping–detrapping diffusion mode, without trap-free diffusion, reveals the electron transport dynamics involved in the backside illumination. The closely-packed EPD films exhibit a shorter electron transit time than does the loosely packed PC films. The porosity dependence of the electron diffusion rate is consistent with the 3D percolation model for metallic solid spheres. The EPD films possess longer electron lifetimes because of their smaller void fraction, which suppresses recombination with electrolytes. The EPD cells, which feature rapid electron transport and suppressed recombination in the TiO_2 films, exhibit a maximum power conversion efficiency of 7.1%, which is higher than that of PC cells (6.0%). Because the distance between electron injection and collection is close to the film thickness and the transport lacks trap-free diffusion, the performance of back-illuminated cells is more sensitive to TiO_2 film thickness and porosity than the performance of the front-illuminated cells. This study demonstrates the advantages of EPD-film architecture in promoting charge collection for high power conversion.

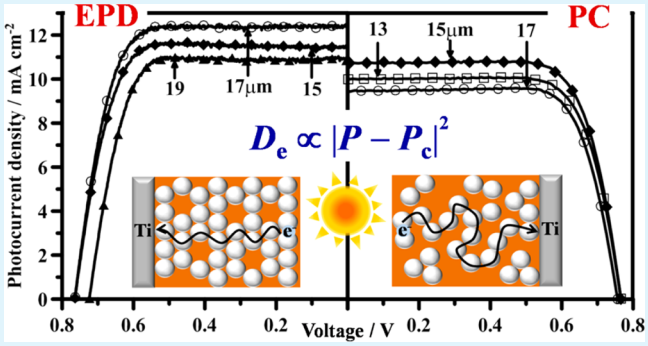

KEYWORDS: *dye-sensitized solar cell, electron transport dynamics, back illumination, electrophoretic deposition*

1. INTRODUCTION

Dye-sensitized solar cells (DSSCs) have been investigated extensively because of their low cost, high efficiency, and environmental friendliness.[1−9] The top-performing DSSCs have reached a power conversion efficiency exceeding 12%.[10] DSSCs typically use glass substrates coated with a transparent conductive oxide for photoelectrodes. Rigid and fragile glass substrates limit the application of DSSCs, particularly as accessories for other equipment and devices. Replacing rigid substrates with flexible substrates extends the application of DSSCs and enables low cost roll-to-roll mass production. Thin and lightweight plastic polymer substrates, such as indium tin oxide (ITO)-coated poly(ethylene terephthalate)[11−14] and ITO-coated poly(ethylene naphthalate)[15−17] substrates, or metal substrates such as Ti, stainless steel, and Zn,[18−23] have been used as flexible substrates for DSSCs. The photovoltaic performance of plastic-based DSSCs is low compared with that of glass-based DSSCs because the high-temperature necking of TiO_2 particles is not applicable to plastic substrates.[13,24,25] Using metal substrates enables the manufacture of high-temperature sintered TiO_2 films for flexible DSSCs with backside illumination. However, the electron transport dynamics associated with this backside illumination configuration have not been adequately explored.

The backside illumination configuration causes considerable incident light loss from scattering by the Pt counter electrode and absorption by the electrolyte. Optimizing the Pt layer thickness and iodide electrolyte concentration is an essential step for achieving a high photovoltaic performance. Backside illumination results in the majority of photogenerated electrons being injected at the edge of the TiO_2 film and produces a longer electron diffusion length relative to that of frontside illumination. Electrophoretic deposition (EPD) of TiO_2 films would be beneficial to back-illuminated DSSCs because it produces a closely packed network of TiO_2 films exhibiting improved electron percolation.[26] In addition, EPD has the

Received: August 31, 2013
Accepted: October 22, 2013
Published: October 22, 2013

advantage of technical reliability and low cost for TiO_2-film fabrication.[27−29]

On the basis of this knowledge, we prepared flexible TiO_2 films by using EPD and paste-coating (PC) of TiO_2 nanoparticles on Ti foils in back-illuminated DSSCs that were optimized for counter Pt thickness and iodide-electrolyte concentration. A series of tests showed that EPD considerably reduced the transit time for electrons generated by blue-light in solar irradiation. In addition, this study suggests that the electron transport dynamics in the TiO_2 films of back-illuminated DSSCs follow the 3D percolation model for metallic solid spheres.

2. EXPERIMENTAL SECTION

The TiO_2 nanoparticles for fabricating the TiO_2 films were synthesized from a titanated-directed method that produces phase-pure anatase.[30−33] In brief, we prepared the TiO_2 nanoparticles by mixing 3 g of commercially available TiO_2 powder (P25, Degussa) with 100 mL of 10 M NaOH (J.T. Baker) and heating the mixture in an autoclave at 130 °C for 20 h. The resulting product was washed with 0.1 M HNO_3 (Showa) to achieve a low pH value of 1.2. The low-pH solution was subjected to a hydrothermal treatment at 240 °C for 12 h to obtain a TiO_2 (approximately 20 nm in size) colloidal solution.

A TiO_2 suspension for EPD was prepared by mixing 3 g of the prepared TiO_2 with 75 mL of ethanol and a small amount of acetyl acetone (Merck) using magnetic stirring for 24 h. A charging solution was obtained by dissolving 268 mg of iodine in a 1000 mL ethanol solution containing 40 mL of acetone and 20 mL of deionized water.[34,35] Immediately prior to EPD, the TiO_2 suspension was added to the charging solution with subsequent sonication for 15 min in an ice bath. We also prepared films by using PC deposition to compare with those fabricated using EPD. The viscous TiO_2 paste for the PC method was obtained by mixing the TiO_2 colloidal solution with poly(ethylene glycol) (PEG; Fluka, 20 000 in molecular weight) at a PEG/TiO_2 ratio of 0.4.[31]

This study used Ti foil substrates (0.25 mm in thickness and 99.7% in purity) to prepare the working electrodes for DSSCs. The substrates were oxidized with 50 mL of 30 wt % hydrogen peroxide solution at room temperature for 48 h before TiO_2 deposition.[36] For EPD film preparation, an oxidized Ti substrate and a fluorine-doped SnO_2 conducting glass substrate (TEC 7, Hartford Glass) were used as the cathodic substrate and counter electrode, respectively. The substrates were placed vertically 0.8 cm apart and immersed in a charged TiO_2 suspension. The EPD process was conducted at a constant voltage in an ice bath. To increase the film thickness and avoid crack formation,[34] we used multistep EPD, consisting of repetitive deposition at 10 V for 20 s with intermediate drying at room temperature. We subjected the EPD films to sintering at 450 °C for 30 min. For PC film preparation, we blade-coated the viscous TiO_2 paste on the oxidized Ti substrates and subsequently calcined the TiO_2-coated substrates at 450 °C for 30 min. The thickness of the films (0.16 cm^{-2} in the active area) was determined by a profilmeter (Alpha Step 500, Tencor).

To prepare a dye-covered TiO_2 film for a DSSC, we immersed a TiO_2 film in a 0.5 mM N719 dye (Solaronix) solution containing 0.5 mM chenodeoxycholic acid in a mixture of acetonitrile and *tert*-buty alcohol at a 1/1 volume ratio at room temperature for 24 h. The counter electrode was fabricated using sputtering to deposit Pt on an indium-doped SnO_2 conducting glass substrate at various thicknesses, which were estimated by measuring the mass of deposited Pt with a quartz crystal balance and then dividing the mass value by the density of Pt and the deposited area. The dye-covered electrode was assembled with the Pt-coated substrate using a 30 μm-thick sandwich-type thermoplastic frame (Surlyn, Dupont). The electrolyte solution for the DSSCs contained 0.05 M LiI (Aldrich), 1.0 M 1-propyl-2,3-dimethylimidazolium iodide (Solarnix), 0.1 M guanidinium thiocyanate (Aldrich), 0.5 M 4-tert-butylpyridine (Aldrich), and I_2 of varying concentrations in a solvent mixture of acetonitrile (J.T. Baker) and valeronitrile (Aerosil) (v/v, 85/15).

For photovoltaic measurements of the DSSCs, an AM 1.5 solar simulator (sp91160A-4739, Newport) was employed for backside irradiation at a light intensity of 100 mW cm^{-2}. The electron transport properties were measured using intensity-modulated photocurrent spectroscopy (IMPS) with a frequency response analyzer (XPOT, Zahner), which also drove a blue light diode (λ = 455 nm) at a DC light intensity of 15 mW cm^{-2} and a red light diode (λ = 625 nm) at 10 mW cm^{-2}. The light intensities were modulated (5%) by adjusting the voltage applied to the diode with sinusoidal waves in a frequency range of $0.1-10^4$ Hz. The electrochemical impedance spectroscopy (EIS) analysis of the cells was conducted with a potentiostat equipped with a frequency response analyzer (IM6, Zahner) over a frequency range of $0.1-10^5$ Hz. The bias potential was set at the open circuit with an AC potential amplitude of 10 mV under an AM 1.5 solar illumination of 100 mW cm^{-2}.

3. RESULTS AND DISCUSSION

In this study, the EPD and PC methods were used to deposit TiO_2 nanoparticles onto Ti foils. Figure S1 of the Supporting Information provides images for comparing the TiO_2 networks that constitute the EPD and PC films. The EPD films exhibited a more compact TiO_2 network than the PC films did. We incorporated these films into back-illuminated DSSCs to compare the electron transport dynamics in TiO_2 films of different porosities.

3.1. Optimization of the Counter Pt Thickness and Iodide-Electrolyte Concentration. In front-illuminated DSSCs, a Pt layer in the range of 2−415 nm exerts only a minor influence on the performance of the cells.[37] In the backside illumination system, the Pt layer of the counter electrode requires high transparency for light penetration.[38,39] Figure S2 of the Supporting Information shows the light transmittance of Pt-coated counter electrodes displaying different Pt thicknesses, and Figure S3 of the Supporting Information displays the photocurrent−voltage characteristics of the resulting DSSCs under AM 1.5 solar illumination from the backside at 100 mW cm^{-2} of light intensity. The influence of the Pt layer thickness on counter electrode properties and, subsequently, on the cell performance through the use of electrochemical impedance spectroscopy (EIS) is further discussed in the Supporting Information (Figure S4 and Table S1).

The performance of back-illuminated cells is affected by the iodide concentration in the redox electrolyte because the iodide species reveals an absorption ability in the visible light spectrum. We varied the I_2 concentration at a fixed LiI concentration (0.05 M) to determine an appropriate electrolyte solution for backside illumination. Figure S5 of the Supporting Information shows the photocurrent−voltage characteristics of the DSSCs possessing varying I_2 concentrations in the electrolyte. On the basis of these preliminary experiments, in this study, the optimal Pt thickness (0.25 nm) and I_2 concentration (0.01 M) were used to assemble DSSCs for further study and discussion of electron transport in TiO_2 films.

3.2. Influence of TiO_2 Thickness on Electron Transport. The electron transport in back-illuminated DSSCs depends heavily on the TiO_2-film thickness because most of the photo-generated electrons travel along the entire film thickness before being collected by the Ti substrates. Figure 1 shows the photocurrent−voltage characteristics of the DSSCs assembled with EPD and PC TiO_2 films of varying thicknesses under AM 1.5 solar illumination at 100 mW cm^{-2}. The EPD

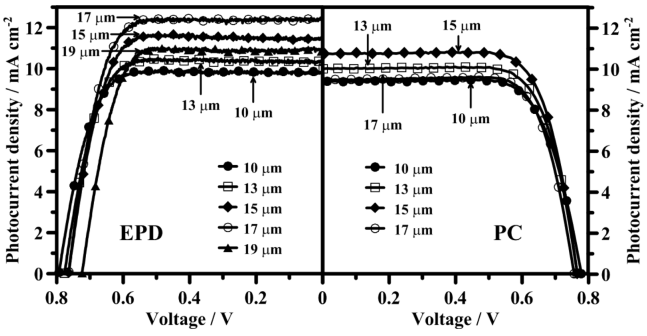

Figure 1. Photocurrent–voltage characteristics of back-illuminated DSSCs assembled with the EPD and PC TiO_2 films of varying thicknesses under AM 1.5 solar illumination at 100 mW cm^{-2}.

cells outperformed the PC cells at each film thickness. Figure 2 shows a summary of the cell performance indices based on the

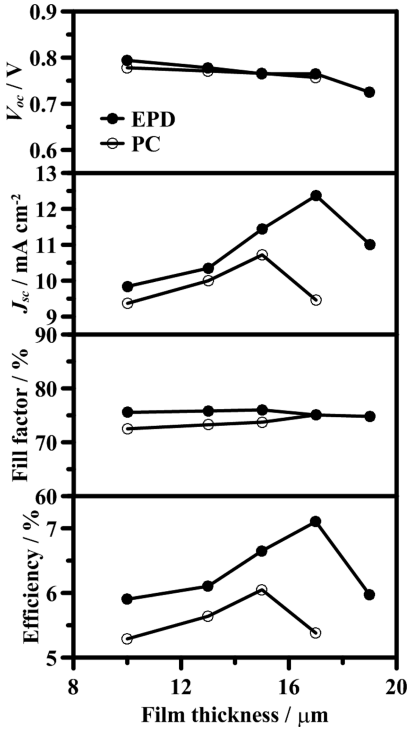

Figure 2. Dependence of cell performances on the film thickness of back-illuminated DSSCs assembled with the EPD and PC films under AM 1.5 solar illumination at 100 mW cm^{-2} light intensity.

data in Figure 1. The open circuit voltage (V_{oc}) decreased when the film thickness increased for both EPD and PC cells. In contrast, the short circuit current (J_{sc}) increased in conjunction with the film thickness to reach its maximal value and then slightly decreased. The fill factor did not reveal obvious variation as the film thickness changed. When these effects were combined, maximal efficiency occurred at thickness levels of 17 and 15 μm for the EPD and PC TiO_2 films, respectively. The J_{sc} values also exhibited maximum efficiency at these film thicknesses. This concurrence suggests that the J_{sc} change governed the cell efficiency variation with the TiO_2 film thickness, whereas the changes in V_{oc} and the fill factor revealed only minor influence. The EPD cells exhibited larger photocurrents than the PC cells did and, consequently, higher conversion efficiencies.

We have measured the amount of dye loaded onto the EPD and PC films (Figure S6 of the Supporting Information). The EPD films have approximately 6% more dye loading than the PC films, while for films 15–17 μm thick the photocurrents of the EPD films exceeded those of the PC by much more than 6%. The dye-loading difference alone cannot account for the great difference between the photocurrents exhibited by these two types of films. Further analysis of electron transport dynamics is necessary to elucidate the superior performance of the EPD cells.

In this study, the cells were subjected to IMPS and EIS analyses to explore the electron transport pattern. IMPS analysis measures the photocurrent response to incident-light density modulation, which consists of a constant-intensity DC illumination, superimposed with a small sinusoidal perturbation.[40−42] The cells were short-circuited during the IMPS measurement. Figure 3 shows the IMPS responses of the EPD

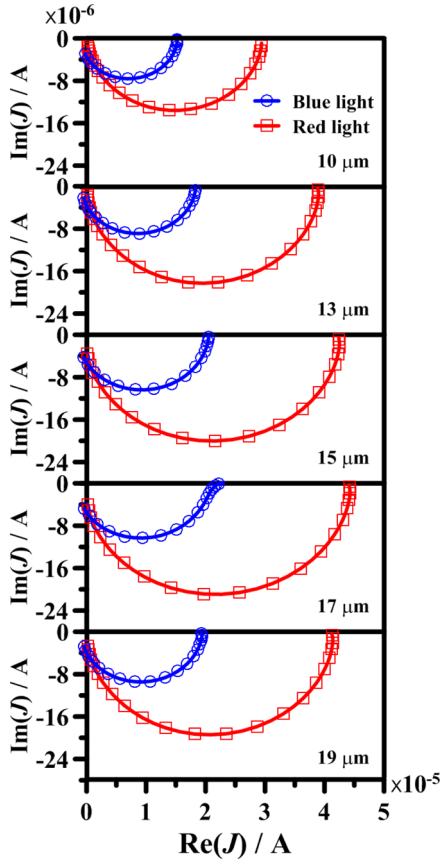

Figure 3. IMPS responses of DSSCs assembled with the EPD TiO_2 films of varying thicknesses under short circuit conditions. Blue (λ = 455 nm) and red (λ = 625 nm) light-emitting diodes were used as the modulation light sources with DC intensities of 15 and 10 mW cm^{-2}, respectively, and superimposed 5% AC intensity.

cells for different film thicknesses with irradiations of blue light (455 nm) at 15 mW cm^{-2} (3.4×10^{20} m^{-2}s^{-1} in photon flux) and red light (625 nm) at 10 mW cm^{-2} (3.1×10^{20} m^{-2}s^{-1} in photon flux). Both the blue-light and red-light irradiations resulted in a one-semicircle feature in the complex-plane spectra at all levels of film thickness. The one-semicircle feature indicates that a single trap-limited diffusion mode (i.e., transport involving the trapping–detrapping process) can describe the entire electron transport. Electron transport in

front-illuminated cells involves both the trap-free and trap-limited diffusion modes[41,42] and results in a two-semicircle feature in the IMPS spectra. The trap-free diffusion mode, with a shorter transit time, corresponds to electron transport through a region with trap states fully filled by electrons.[41] Figure 3 shows that the size of the semicircles increased when the film thickness increased and reached a maximal value at a thickness of 17 μm. The photon fluxes of the blue-light and red-light irradiations were similar, whereas the photocurrents (the ultimate $Re(J)$ values) induced by the red light were larger than those induced by the blue light for all TiO_2-film thicknesses, although the N719 dye exhibits a stronger propensity to absorb blue light. The difference between the photocurrents from red and blue irradiations increased when the film thickness increased, indicating that red-light conversion predominantly accounted for the cell-efficiency increase with film thickness, as shown in Figure 2.

Figure 4 provides a schematic for elucidating the photocurrent difference resulting from the different light irradiations.

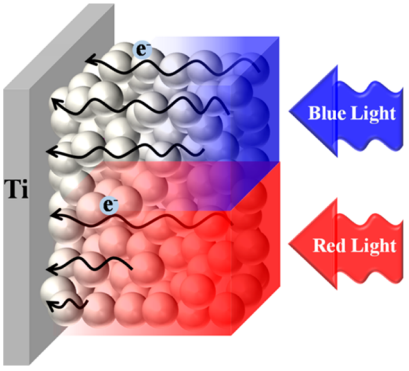

Figure 4. Schematic showing the light-harvesting distributions on TiO_2 films for light irradiations of different wavelengths from the counter-electrode side of DSSCs.

Because the extinction coefficient of the dye is large in the blue,[2] the strongly absorbing blue light generates electrons primarily on the illuminated side of the TiO_2 film. Red light is weakly absorbed by the dye, and electrons are generated more uniformly throughout the film.[26,42] In the case of thinner TiO_2 films, the positions of charge generation for both the blue-light and red-light irradiations are close to the collector foil, thereby resulting in a smaller difference between the photocurrents from different irradiations. However, in the case of the thicker TiO_2 films, the electrons generated by blue light must travel a long distance before collection, leading to a high probability of charge-recombination loss.[2,41,42] Most of the incident photons, either the blue or red, are absorbed by thick dyed-TiO_2 films. The difference in the electron travel distance explains why using red light leads to a higher photocurrent than using blue light in back-illuminated DSSCs. In contrast, our previous study has shown that front-illuminated DSSCs exhibit a higher photon conversion efficiency with blue light compared to that with red light.[26]

Figure 5 shows the IMPS responses of the PC cells for various film thicknesses under blue-light and red-light irradiations. The induced photocurrents are smaller than those of the EPD cells, particularly for the currents induced by red light. We calculated the electron transit time (τ_d) from the IMPS measurements by using the relation $\tau_d = (2\pi f_{min})^{-1}$, where f_{min} is the characteristic frequency minimum of the

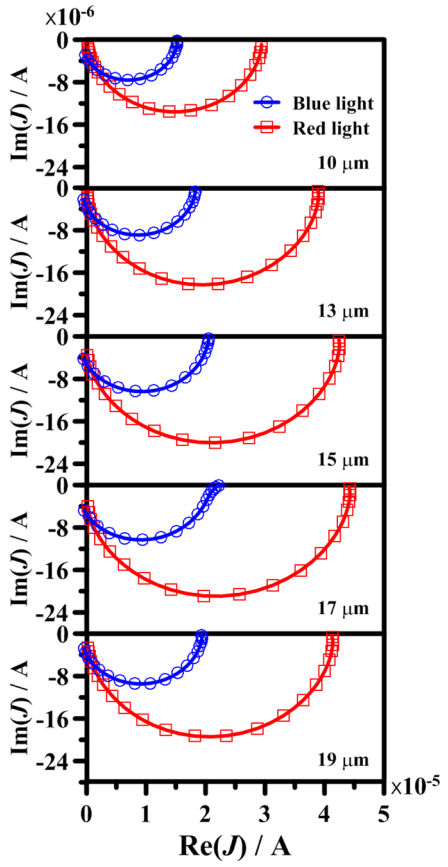

Figure 5. IMPS responses of DSSCs assembled with the PC TiO_2 films of varying thicknesses under short circuit conditions. Blue (λ = 455 nm) and red (λ = 625 nm) light-emitting diodes were used as the modulation light sources with DC intensities of 15 and 10 mW cm^{-2}, respectively, and superimposed 5% AC intensity.

imaginary component of the semicircles in the spectra.[40,43−45] Figure 6 provides a summary of the trap-limited electron transit time in the back-illuminated DSSCs. The electron transit time increased when the film thickness increased because of the increase in length of the electron diffusion path. The electron transit time of the EPD cells was shorter than that of the PC cells because the compact EPD films exhibited a smaller tortuosity value for the electron diffusion path.[26] Red light illumination generates uniform electron injection into TiO_2 films for both back- and front-illuminated configurations. The transit time of the back-illuminated EPD cells (e.g., 9 ms with a 10 μm film under red-light irradiation) was longer than that of the front-illuminated EPD cells (8 ms).[26] The difference in the cells assembled with a 10 μm PC film was even larger, with transit times of 20 and 10 ms for the back- and front-illuminated cells, respectively. This demonstrates the advantage of using EPD films for back-illuminated cells.

To further reveal the influence of the TiO_2-film structure on electron transport characteristics under backside illumination, we subjected the cells to EIS analysis, using a one-sun illumination (100 mW cm^{-2}).[46−48] Figure 7 shows the Nyquist impedance spectra of the back-illuminated cells in the open-circuit condition. This EIS analysis focused on the middle-frequency arc that relates to electron transport in TiO_2 film. We simulated the spectra with a transmission line model (Figure S4b of the Supporting Information),[49−52] in which the elements of the circuit relating to TiO_2 films were the electron

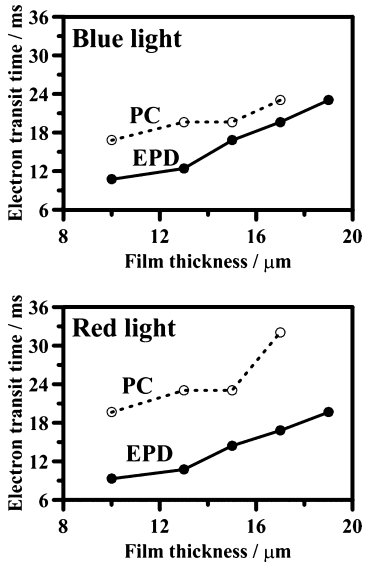

Figure 6. Effect of TiO_2 film thickness on the electron transit time for the EPD and PC cells based on the IMPS analyses under blue- and red-light illuminations. The transit times were obtained by the f_{min} of the IMPS plots. The incident DC illumination intensities were 15 mW cm^{-2} for blue light and 10 mW cm^{-2} for red light.

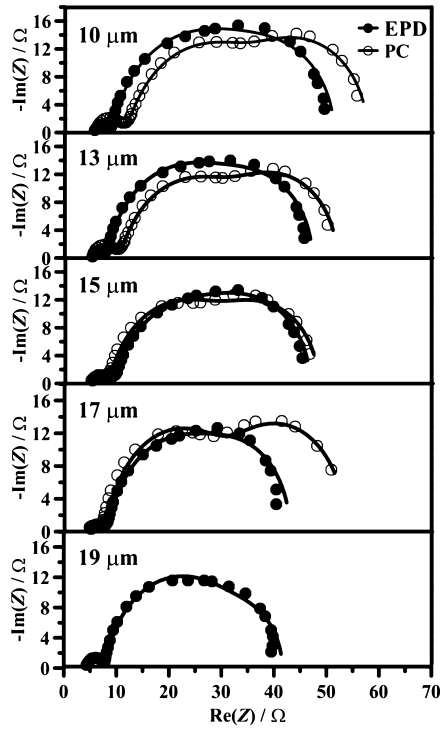

Figure 7. Nyquist impedance plots of DSSCs assembled with the EPD and PC TiO_2 films of varying thicknesses under AM 1.5 solar illumination at 100 mW cm^{-2}, with the AC frequency ranging from 0.1 to10^5 Hz at the open-circuit voltage of the cells. The solid lines represent the results simulated using the parameters in Table 1.

transport resistance, R_t ($=r_tL$), the interfacial charge recombination resistance, R_{ct} ($=r_{ct}/L$), and the chemical capacitance produced by the accumulation of electrons in the TiO_2 film, C_μ ($=c_\mu L$), where L is the TiO_2 film thickness. Table 1 displays the values of c_μ, r_t, and r_{ct} obtained from the simulation. The mean electron transit time, $\tau_{d,EIS}$, can be determined from the equation $\tau_{d,EIS} = r_t \times c_\mu \times L^2$. Table 1 presents the values of $\tau_{d,EIS}$. The more compact EPD films exhibited smaller r_t and $\tau_{d,EIS}$ for electron transport. This is consistent with the results of IMPS measurements, which showed shorter transit times in the EPD films.

Table 1. Equivalent-Circuit Parameters of DSSCs Assembled with the EPD and PC TiO_2 Films of Varying Thicknesses and the Electron Diffusion Coefficient (D_e) in the TiO_2 Films[a]

L/ μm	c_μ/ μF μm^{-1}	r_t/ Ω μm^{-1}	r_{ct}/ Ω μm	$\tau_{d,EIS}$/ ms	$\tau_{n,EIS}$/ ms	D_e/cm^2 s^{-1}
			EPD Cells			
10	148	0.14	227	2.12	33.6	4.72×10^{-4}
13	149	0.14	231	3.10	34.5	4.65×10^{-4}
15	139	0.15	248	4.75	34.4	4.73×10^{-4}
17	139	0.15	294	6.23	41.0	4.64×10^{-4}
19	144	0.17	336	7.68	43.7	4.36×10^{-4}
			PC Cells			
10	96.9	0.38	203	3.70	19.7	2.05×10^{-4}
13	108	0.35	254	4.93	24.2	2.63×10^{-4}
15	105	0.30	276	7.17	29.0	3.14×10^{-4}
17	110	0.33	315	10.5	34.7	2.75×10^{-4}

[a]Values are determined on the basis of the data of Figure 7.

Conducting the EIS analysis, we calculated the electron diffusion coefficient (D_e) of the TiO_2 films by following $D_e = L^2/\tau_{d,EIS} = (r_t \times c_\mu)^{-1}$ and listed the values in Table 1. The D_e value does not show significant variation with the film thickness because the trap density does not vary with L.[41] However, in the front-illuminated cells, the D_e value increases with L because of the increased contribution of the trap-free diffusion mode for electrons that neighbor the collector.[26] Table 1 shows that the closely-packed EPD films possessed larger D_e values than did the loosely-packed PC films. We correlated D_e and the porosity (P) of the films from the pore volume by using a power-law relationship: $D_e \propto |P - P_c|^\beta$, where P_c is the critical porosity (0.76, according to ref 53) and β is the power-law exponent. The P values of the PC and EPD films were 0.61 and 0.54, respectively.[26] The back-illuminated TiO_2 films show a β value approximately equal to 2, which is consistent with the conductive exponent for a 3D percolation model. This concurrence indicates that the electron transport patterns in the PC and EPD films are microscopically similar and that the porosity governs the transport dynamics. For front illumination, the β value was smaller than 2 in most cases.[26,53] We attribute this β-value reduction to the presence of the trap-free diffusion zone in front-illuminated cells because the trap-free diffusion affects the apparent D_e value.

The competition between forward transport and back recombination governs the collection efficiency of the photogenerated electrons. We calculated the mean electron lifetime in TiO_2 from the relation $\tau_{n,EIS} = r_{ct} \times c_\mu$ and listed the data in Table 1. The compact EPD films have greater $\tau_{n,EIS}$ than the PC films. The smaller void fraction of the EPD films may have suppressed the recombination tendency and, therefore, increased $\tau_{n,EIS}$. The electron collection rate at the Ti foil substrate is obtained by subtracting the recombination rate from the forward diffusion rate:

$$\frac{1}{\tau_{cc}} = \frac{1}{\tau_{d,EIS}} - \frac{1}{\tau_{n,EIS}} \quad (1)$$

where τ_{cc} is the time constant for electron collection. Accordingly, the electron collection efficiency can be written as[54,55]

$$\eta_{cc} = \frac{1}{\tau_{cc}} \Big/ \left(\frac{1}{\tau_{cc}} + \frac{1}{\tau_{n,EIS}}\right) = 1 - \frac{\tau_{d,EIS}}{\tau_{n,EIS}} = 1 - \frac{r_t}{r_{ct}} L^2 \quad (2)$$

Figure 8 shows the film thickness dependence of the electron collection efficiency. The η_{cc} values of the EPD films are larger

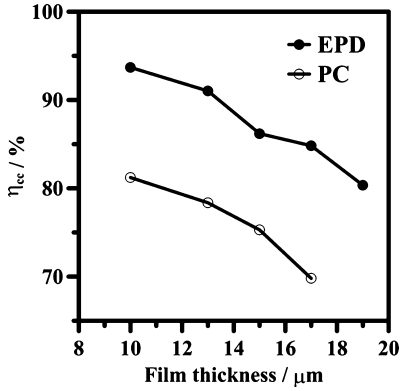

Figure 8. Dependence of charge collection efficiency (η_{cc}) on the film thickness for back-illuminated DSSCs assembled with the EPD and PC TiO_2 films.

than those of the PC films because of the effective forward transport (smaller $\tau_{d,EIS}$) and limited recombination (larger $\tau_{n,EIS}$) of the EPD films.

The highest electron collection efficiency occurs at the thinnest TiO_2 films for both EPD and PC films and decreases when the film thickness increases. Increasing the electron transport path promotes the probability of losing electrons by recombination. Our previous study revealed that the η_{cc} value of front-illuminated EPD cells remained at 95% for film thicknesses up to 13 μm.[26] The present study revealed a sharp decrease in the η_{cc} value when the film thickness increased. This difference occurred primarily because, in backside illumination, the majority of photogenerated electrons must travel through the entire film before being collected, and the charge collection is sensitive to the film thickness. In front-illuminated cells, the majority of electrons exhibit a short travelling path because they are injected near the collector, and electron transport involves the trap-free diffusion mode that is advantageous for electron transport and collection for thicker TiO_2 films.[41,42] The charge collection efficiency was not sensitive to film thickness for front-illuminated cells. In contrast, Figure 8 demonstrates the importance of compact films in charge collection for the back-illuminated cells.

4. CONCLUSIONS

In back-illuminated DSSCs, a large proportion of photogenerated electrons travel through the entire TiO_2 film for charge collection, rendering the collection efficiency highly sensitive to the film thickness and porosity. The electrons generated by weakly absorbing red light inject uniformly into TiO_2 films and have a shorter mean travel distance than those by blue light. Red-light conversion predominantly accounted for the conversion efficiency increase when the film thickness increased in back-illuminated DSSCs.

The electron transport dynamics in back-illuminated cells involved only a single trap-limited diffusion mode, which differs from those in front-illuminated cells that involved both the trap-free and trap-limited diffusion modes. The closely-packed EPD films exhibited greater D_e values than did the loosely-packed PC films. Because of lacking trap-free diffusion, the electron transport dynamics in the back-illuminated TiO_2 films were consistent with the 3D percolation model for metals. The effective forward transport (greater D_e) and limited recombination (longer $\tau_{n,EIS}$) resulted in a higher charge collection efficiency of EPD films relative to that of conventional PC films.

The back-illuminated configuration exhibited a drastic decay in charge collection efficiency when the film thickness increased because of the vast separation between electron injection and collection and the absence of trap-free diffusion. The electron diffusion rate in back-illuminated TiO_2 films exhibited a stronger dependence on the film porosity than that in front-illuminated films. The EPD technique that produces closely-packed TiO_2 films is particularly suitable for fabricating back-illuminated DSSCs.

■ ASSOCIATED CONTENT

Ⓢ Supporting Information

Top-view SEM images of the EPD and PC TiO_2 films; light transmittance of Pt-coated counter electrodes with different Pt thicknesses; photocurrent−voltage characteristics and EIS analysis of the DSSCs with different Pt thicknesses; photocurrent−voltage characteristics and EIS analysis of the DSSCs with varying I_2 concentrations in the electrolyte; amounts of dye loaded onto the TiO_2 films. This information is available free of charge via the Internet at http://pubs.acs.org.

■ AUTHOR INFORMATION

Corresponding Authors

*E-mail: hteng@mail.ncku.edu.tw. Fax: 886-6-2344496. Tel: 886-6-2385371 (H. Teng).

*E-mail: cthsieh@saturn.yzu.edu.tw (C.-T. Hsieh).

Notes

The authors declare no competing financial interest.

■ ACKNOWLEDGMENTS

This research is supported by the National Science Council of Taiwan (101-2221-E-006-243-MY3, 101-2221-E-006-225-MY3, 102-3113-P-006-012, and 102-3113-E-006-002) and the "Aim for the Top-Tier University and Elite Research Center Development Plan" of National Cheng Kung University.

■ REFERENCES

(1) O'Regan, B.; Grätzel, M. *Nature* **1991**, *353*, 737−740.
(2) Nazeeruddin, M. K.; Kay, A.; Rodicio, I.; Humphry-Baker, R.; Müller, E.; Liska, P.; Vlachopoulos, N.; Grätzel, M. *J. Am. Chem. Soc.* **1993**, *115*, 6382−6390.
(3) Grätzel, M. *Nature* **2001**, *414*, 338−344.
(4) Peter, L. M. *Phys. Chem. Chem. Phys.* **2007**, *9*, 2630−2642.
(5) Grätzel, M. *J. Photochem. Photobiol., A* **2004**, *164*, 3−14.
(6) Chen, C. Y.; Wang, M.; Li, J. Y.; Pootrakulchote, N.; Alibabaei, L.; Ngoc-le, C. H.; Decoppet, J. D.; Tsai, J. H.; Grätzel, C.; Wu, C. G.; Zakeeruddin, S. M.; Grätzel, M. *ACS Nano* **2009**, *3*, 3103−3109.
(7) Das, J.; Freitas, F. S.; Evans, I. R.; Nogueira, A. F.; Khushalani, D. *J. Mater. Chem.* **2010**, *20*, 4425−4431.
(8) Tang, Y. B.; Lee, C. S.; Xu, J.; Liu, Z. T.; Chen, Z. H.; He, Z.; Cao, Y. L.; Yuan, G.; Song, H.; Chen, L.; Luo, L.; Cheng, H. M.; Zhang, W. J.; Bello, I.; Lee, S. T. *ACS Nano* **2010**, *4*, 3482−3488.

(9) Adachi, M.; Tanino, R.; Adachi, J.; Mori, Y.; Tsuchiya, K.; Isoda, S.; Uchida, F. *J. Power Sources* **2013**, *226*, 94−100.
(10) Yella, A.; Lee, H. W.; Tsao, H. N.; Yi, C.; Chandiran, A. K.; Nazeeruddin, M. K.; Diau, W.G.; Yeh, C. Y.; Zakeeruddin, S. M.; Grätzel, M. *Science* **2011**, *334*, 629−634.
(11) Lindström, H.; Holmberg, A.; Magnusson, E.; Lindquist, S. E.; Malmqvist, L.; Hagfeldt, A. *Nano Lett.* **2001**, *1*, 97−100.
(12) Haque, S. A.; Palomares, E.; Upadhyaya, H. M.; Otley, L.; Potter, R. J.; Holmes, A. B.; Durrant, J. R. *Chem. Commun.* **2003**, *24*, 3008−3009.
(13) Miyasaka, T.; Kijitori, Y. *J. Electrochem. Soc.* **2004**, *151*, A1767−A1773.
(14) Nogueira, A. F.; Longo, C.; De Paoli, M. A. *Coord. Chem. Rev.* **2004**, *248*, 1455−1468.
(15) Shin, K.; Jun, Y.; Moon, J. H.; Park, J. H. *ACS Appl. Mater. Interfaces* **2010**, *2*, 288−291.
(16) Lee, K. M.; Wu, S. J.; Chen, C. Y.; Wu, C. G.; Ikegami, M.; Miyoshi, K.; Miyasaka, T.; Ho, K. C. *J. Mater. Chem.* **2009**, *19*, 5009−5015.
(17) Chen, L. C.; Ting, J. M.; Lee, Y. L.; Hon, M. H. *J. Mater. Chem.* **2012**, *22*, 5596−5601.
(18) Kang, M. G.; Park, N. G.; Ryu, K. S.; Chang, S. H.; Kim, K. J. *Chem. Lett.* **2005**, *34*, 804−805.
(19) Chen, H. W.; Huang, K. C.; Hsu, C. Y.; Lin, C. Y.; Chen, J. G.; Lee, C. P.; Lin, L. Y.; Vittal, R.; Ho, K. C. *Electrochim. Acta* **2011**, *56*, 7991−7998.
(20) Liao, J. Y.; Lei, B. X.; Chen, H. Y.; Kuang, D. B.; Su, C. Y. *Energy Environ. Sci.* **2012**, *5*, 5750−5757.
(21) Chung, K. H.; Rahman, M. M.; Son, H. S.; Lee, J. J. *Int. J. Photoenergy* **2012**, *2012*, 215802.
(22) Yun, H. G.; Jun, Y.; Kim, J.; Bae, B. S.; Kang, M. G. *Appl. Phys. Lett.* **2008**, *93*, 133311.
(23) Miettunen, K.; Halme, J.; Toivola, M.; Lund, P. *J. Phys. Chem. C* **2008**, *112*, 4011−4017.
(24) Lindström, H.; Holmberg, A.; Magnusson, E.; Malmqvist, L.; Hagfeldt, A. *J. Photochem. Photobiol., A* **2001**, *145*, 107−112.
(25) Yamaguchi, T.; Tobe, N.; Matsumoto, D.; Nagai, T.; Arakawa, H. *Sol. Energy Mater. Sol. Cells* **2010**, *94*, 812−816.
(26) Liou, Y. J.; Hsiao, P. T.; Chen, L. C.; Chu, Y. Y.; Teng, H. S. *J. Phys. Chem. C* **2011**, *115*, 25580−25589.
(27) Zhitomirsky, I.; Petric, A. *Mater. Lett.* **1999**, *40*, 263−268.
(28) Hosseinbabaei, F.; Raissidehkordi, B. *J. Eur. Ceram. Soc.* **2000**, *20*, 2165−2168.
(29) Zhitomirsky, I. *Adv. Colloid Interface Sci.* **2002**, *97*, 279−317.
(30) Nian, J. N.; Teng, H. S. *J. Phys. Chem. B* **2006**, *110*, 4193−4198.
(31) Hsiao, P. T.; Wang, K. P.; Cheng, C. W.; Teng, H. S. *J. Photochem. Photobiol., A* **2007**, *188*, 19−24.
(32) Tsai, C. C.; Teng, H. S. *Chem. Mater.* **2006**, *18*, 367−373.
(33) Tsai, C. C.; Teng, H. S. *Langmuir* **2008**, *24*, 3434−3438.
(34) Grinis, L.; Dor, S.; Ofir, A.; Zaban, A. *J. Photochem. Photobiol., A* **2008**, *198*, 52−59.
(35) Dor, S.; Ruhle, S.; Ofir, A.; Grinis, L.; Zaban, A. *Colloids Surf., A* **2009**, *342*, 70−75.
(36) Lee, C. H.; Chiu, W. H.; Lee, K. M.; Hsieh, W. F.; Wu, J. M. *J. Mater. Chem.* **2011**, *21*, 5114−5119.
(37) Fang, X.; Ma, T.; Guan, G.; Akiyama, M.; Kida, T.; Abe, E. *J. Electroanal. Chem.* **2004**, *570*, 257−263.
(38) Onoda, K.; Ngamsinlapasathian, S.; Fujieda, T.; Yoshikawa, S. *Sol. Energy Mater. Sol. Cells* **2007**, *91*, 1176−1181.
(39) Lina, L. Y.; Lee, C. P.; Vittal, R.; Ho, K. C. *J. Power Sources* **2010**, *195*, 4344−4349.
(40) Fisher, A. C.; Peter, L. M.; Ponomarev, E. A.; Walker, A. B.; Wijayantha, K. G. U. *J. Phys. Chem. B* **2000**, *104*, 949−958.
(41) Hsiao, P. T.; Tung, Y. L.; Teng, H. S. *J. Phys. Chem. C* **2010**, *114*, 6762−6769.
(42) Hsiao, P. T.; Liou, Y. J.; Teng, H. S. *J. Phys. Chem. C* **2011**, *115*, 15018−15024.
(43) Franco, G.; Gehring, J.; Peter, L. M.; Ponomarev, E. A.; Uhlendorf, I. *J. Phys. Chem. B* **1999**, *103*, 692−698.
(44) Krüger, J.; Plass, R.; Grätzel, M.; Cameron, P. J.; Peter, L. M. *J. Phys. Chem. B* **2003**, *107*, 7536−7539.
(45) Kopidakis, N.; Benkstein, K. D.; van de Lagemaat, J.; Frank, A. J. *J. Phys. Chem. B* **2003**, *107*, 11307−11315.
(46) Kern, R.; Sastrawan, R.; Ferber, J.; Stangl, R.; Luther, J. *J. Electrochim. Acta* **2002**, *47*, 4213−4225.
(47) Adachi, M.; Sakamoto, M.; Jiu, J.; Ogata, Y.; Isoda, S. *J. Phys. Chem. B* **2006**, *110*, 13872−13880.
(48) Hoshikawa, T.; Yamada, M.; Kikuchi, R.; Eguchi, K. *J. Electrochem. Soc.* **2005**, *152*, E68−E73.
(49) Bisquert, J. *J. Phys. Chem. B* **2002**, *106*, 325−333.
(50) Fabregat-Santiago, F.; Bisquert, J.; Palomares, E.; Otero, L.; Kuang, D.; Zakeeruddin, S. M.; Grätzel, M. *J. Phys. Chem. C* **2007**, *111*, 6550−6560.
(51) Wang, K. P.; Teng, H. S. *J. Phys. Chem. Chem. Phys.* **2009**, *11*, 9489−9496.
(52) Wang, M.; Chen, P.; Humphry-Baker, R.; Zakeeruddin, S. M.; Grätzel, M. *ChemPhysChem* **2009**, *10*, 290−299.
(53) Benkstein, K. D.; Kopidakis, N.; van de Lagemaat, J.; Frank, A. J. *J. Phys. Chem. B* **2003**, *107*, 7759−7767.
(54) Wang, Q.; Ito, S.; Grätzel, M.; Febregat-Santiago, F.; Mora-Seró, I.; Bisquert, J.; Bessho, T.; Imai, H. *J. Phys. Chem. B* **2006**, *110*, 25210−25221.
(55) van de Lagemaat, J.; Park, N. G.; Frank, A. J. *J. Phys. Chem. B* **2002**, *104*, 2044−2052.